How the Three Gorges Project (TGP) affects local precipitation

Qin Li[1], Yulong Zhong[1], Xiuguo Liu[1], Mengmeng Wang[1], and Manxing Shi[1]

[1]School of Geography and Information Engineering, China University of Geosciences, Wuhan, China.

Corresponding author: Y.Zhong (zhongyl@cug.edu.cn) , X.Liu (liuxg318@163.com)

Key Points:

- TGD has influence on the local precipitation.
- After the impoundment of the TGD, the precipitation became increasingly uniform throughout the year.
- An obvious resonance phenomenon between the monthly average water level and precipitation anomaly occurred in the TGRA after 2011 and showed a positive correlation.

Abstract

As the largest hydroelectric projects worldwide, the Three Gorges Dam (TGD) affects local precipitation because of the changes of hydrological cycle caused by the impounding and draining of the TGD. However, the influencing characteristics of the TGD on local precipitation remain elusive. In this study, we used precipitation anomaly data derived from long time-series grid precipitation datasets between 1988 and 2017 to understand the changes of precipitation caused by the TGD between 2 epochs, before and after the construction of the TGD (i.e., 1988–2002 and 2003–2017), in the Three Gorges Reservoir Area (TGRA). Results showed that the annual and dry season precipitation anomaly in the TGRA showed an increasing trend, and the flood season precipitation anomaly showed a slight decrease. After the impoundment of the TGD, the precipitation concentration degree in the TGRA was decreased, indicating that the precipitation became increasingly uniform, and the precipitation concentration period was insignificantly increased. An obvious resonance phenomenon between the monthly average water level and precipitation anomaly occurred in the TGRA after 2011 and showed a positive correlation. Our findings excavated the change of local precipitation characteristics before and after the impoundment of the TGRA and proved that this change had a close relationship with the water level.

1 Introduction

As an important infrastructure, dams provide numerous conveniences for people's life and production and make a considerable contribution to economic construction (Woldemichael et al., 2012). In addition to their enormous societal benefits, with the construction of a dam, more lands are converted to surface water. This change can lead to the increased availability of local moisture and significantly affect mesoscale circulation (Hossain, 2010; Niyogi et al., 2010). Given that mesoscale circulation is essentially "local" ranging from 10 km to 100 km, one of the local effects on this change can be modification of precipitation (Degu et al., 2011).

The Three Gorges Project (TGP) is one of the world's largest and most functional hydroelectric hub project. The Three Gorges Dam (TGD) brings abundant social and economic benefits, such as electricity generation, flood control, and shipping access (Zheng et al., 2020). Moreover, the increase of the underlying surface area of the water body and the climate change of the large-scale background field lead to changes in the frequency and characteristics of local meteorological disasters (Beatty et al., 2017; Song et al., 2017; Woldemichael et al., 2012). What the influence is of the TGD on local climate and the probable effect on precipitation patterns have attracted widely attention.

Some studies have suggested that the impoundment of the TGD can slightly affect local meteorological conditions, such as temperature and precipitation in the Three Gorges Reservoir Area (TGRA) (Li et al., 2017, 2019; Miller et al., 2005; Wu et al., 2012; Xiao et al., 2010; Zeng et al., 2019). However, some studies have proposed different conclusions. Wu et al. (2006) showed that the impoundment of the TGD will cause a decrease in precipitation near the dam and an increase in precipitation to the north and west of the dam, which may have affected the climate on a regional scale. Fang et al. (2010) discovered significant decreases in spring, fall, winter, and annual number of rainy days and significant increases in precipitation intensity in the TGRA.

The different findings in previous studies may be resulted from several reasons. First, most of the experimental data used in previous studies have been achieved by satellite. Satellite observation has many advantages, such as wide spatial coverage, independent of geographical conditions, continuous observation time, and all-weather observation (Manz et al., 2016; Zhang et al., 2015). However, satellite-based precipitation data are measured indirectly, which is easily limited by sensor property, cloud characteristics, and inversion algorithm. The precipitation monitoring accuracy still needs improvement (Tang et al., 2016; Wang et al., 2017; Wang et al., 2018). Second, most of previous studies have only analyzed a relatively short time period, which did not cover the TGP's entire impounding period from 2003 to 2010 and the stable operation period after 2011. The long time-series precipitation changes before 2003 were also not considered. Therefore, the short period limits the reliability and accuracy of the results and conclusion. In addition, previous scholars have focused on annual and seasonal changes in precipitation, while without considering the precipitation concentration degree (PCD) and the precipitation concentration period (PCP). However, PCD and PCP can quantitatively analyze the basic characteristics and formation mechanism of drought and flood disasters (Abolverdi et al., 2016; Li et al., 2011; Yesilirmak and Atatanir, 2016). Therefore, understanding the changes in PCD and PCP is important to analyze the effect of the TGP on regional climate and the environment. Third, since the TGRA was utilized, the water level in the reservoir area has been changing constantly, but few studies have focused on the relationship between water level and precipitation

Long time-series meteorological grid data have advantages of high precision, wide coverage, long time span, and easy access and processing. Such data provide an opportunity for monitoring the long time-series climate change (Beck et al., 2017; Miao and Wang, 2020; Singh and Qin, 2019; Sun and Wang, 2017). Therefore, long time-series meteorological grid data can provide accurate information for us to analyze the precipitation changes before and after the impoundment of the TGRA. However, the accuracy of different grid datasets is varied in different areas; thus, before using datasets, their accuracy must be initially verified (Yang et al., 2017).

In this study, we evaluated the accuracy of three sets of China's regional long time-series meteorological grid data in the TGRA based on the station data provided by the Hubei Meteorological Bureau. Then, we studied the change in precipitation, the PCD, and the PCP before and after the impoundment in the TGRA. We also analyzed the relationship between precipitation and water level change in the TGRA. This study would provide effective information for local agricultural and production activities in response to local climate change caused by man-made dams.

2 Study Area

The TGRA refers to the area that has been flooded after the completion of the TGD, as shown in Figure 1. The TGRA is located between 28°31′N–31°44′N and 105°50′E–111°40′E. The range of elevation is −22 m to 2991 m. The length of the reservoir is about 660 km, and the average width is approximately 1.1 km. The reservoir can store 39.3 billion m^3 water, which covers about 1084 km^2. Most of the Yangtze River area from Chongqing to Yichang can be controlled by the TGP.

Since the TGD was put into operation in 2003, the water level has risen from 66 m to 175 m. In 2006, 156 m of water storage target was reached, and the 175 m target was completed in September 2010. Then, the water level remained at 175 m in the conventional stage. In

November 2020, the TGP completed the overall completion and acceptance of all procedures. With the change of water level, the water area changes accordingly, increasing from 408 km^2 at the original level of 69 m to 453, 718, and 1062 km^2 when the water level is at 135, 156, and 175 m, respectively (Song et al., 2017).

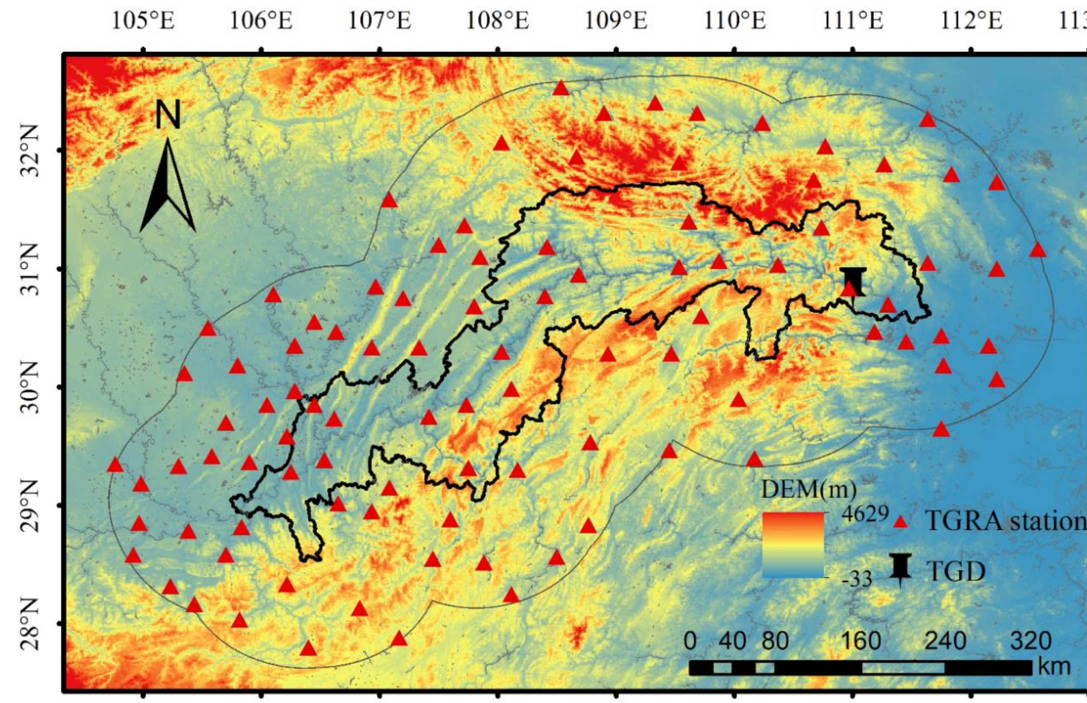

Figure 1. Study area with terrain. Black pin marks the TGD; the thick black line delineates the boundary of the TGRA; the thin black line represents the 1° buffer of the TGRA. Meteorological stations used in this study located within 1° buffer of the TGRA are marked as red triangles.

3 Data and Methods

3.1 Data

We used three classes of data in this study: 1) China's regional meteorological grid data, including 1-km monthly precipitation dataset, CN05.1, China Meteorological Forcing Dataset (CMFD) for China; 2) observation data from 97 meteorological stations in the 1° buffer zone of the TGRA, which helps in selecting the most accurate dataset in the TGRA and analyzing the changes in PCD and PCP; and 3) the water level data in the TGRA, which were used to analyze the relationship between precipitation and water level.

3.1.1. Long time-series meteorological grid data

The 1-km monthly precipitation dataset for China (hereinafter, "1-km dataset") is a dataset that includes monthly air temperatures at 2 m (minimum, maximum, and mean proxy monthly temperatures) and precipitation for China in the period of 1901–2017 on 0.0083333° (equivalent to 1 km) grid. The dataset was spatially downscaled from the 300 Climatic Research Unit time-series dataset with the climatology dataset of WorldClim using delta spatial downscaling (Peng et al., 2019).

CN05.1 is a grid dataset with a resolution of 0.25° × 0.25° from 1961 to 2018 produced by the National Climate Center in China (Wu and Gao, 2013). These data were interpolated based on more than 2400 meteorological stations over China. An “anomaly approach” was applied in the interpolation step. The meteorological elements of CN05.1 dataset includes average temperature, precipitation, maximum temperature, minimum temperature, average wind speed, and relative humidity. With inclusion of more meteorological stations, the CN05.1 data are more reliable than previous versions, which were based on about 700 meteorological stations (Zhang et al., 2014). In this study, we used the monthly precipitation data of CN05.1.

The CMFD is a near-surface meteorological and environmental reanalysis dataset provided by the Institute of Tibetan Plateau Research at the Chinese Academy of Science (He et al., 2020). The dataset is based on Princeton reanalysis data, GEWEX-SRB, GLDAS, and TRMM precipitation data, combined with meteorological data from the China Meteorological Administration (CMA). Observation data from 740 meteorological stations in the CMA were used to correct systematic departures in the background data. The spatial resolution of CMFD is 0.1° with a temporal coverage from 1979 to 2018.

3.1.2. Station precipitation data

The ground meteorological station precipitation data used in our experiment were obtained by the CMA. The dataset includes monthly precipitation data of 97 stations in a 1° buffer zone of the TGRA from 1988 to 2017, such as Yichang, Badong, Fengjie, and Shapingba. The seasonal and annual data were achieved by accumulating the monthly precipitation. The corresponding grid of different grid products was determined based on the latitude and longitude of the station. Figure 1 shows the spatial distribution of these sites.

3.1.3. Water level data

The daily water level data of the TGRA from 2003.5.1 to 2017.12.31 were provided by the Hubei Hydrology and Water Resources Center (http://slt.hubei.gov.cn/sw/). Monthly average water level data were calculated from daily water level data.

3.2 Methods

3.2.1 Accuracy evaluation of different precipitation datasets

In this study, we used the same method as previous studies to evaluate the accuracy of different datasets (Hu et al., 2018; Yang et al., 2017). Two indices were used to evaluate the accuracy of different precipitation datasets (1) The correlation coefficient (CC) can quantify the linear correlation between different grid datasets and station data, and (2) the root mean square error (RMSE) helps quantify the dispersion between different grid datasets and station precipitation data. The existing research results showed that high precision data present low RMSE and high CC. These indices are calculated as follows:

$$CC = \frac{\sum_{i=1}^{n}\left(X_i - \overline{X_{\mathrm{i}}}\right)\left(Y_i - \overline{Y_{\mathrm{i}}}\right)}{\sqrt{\sum_{i=1}^{n}\left(X_i - \overline{X_{\mathrm{i}}}\right)^2 \sum_{i=1}^{n}\left(Y_i - \overline{Y_{\mathrm{i}}}\right)^2}} \qquad (1)$$

$$RMSE = \sqrt{\frac{1}{n}\sum_{i=1}^{n}(X_i - Y_i)^2} \quad (2)$$

where n is the number of data points included in the comparison, X_i is an element of the evaluated dataset, $\overline{X_i}$ is the average value for the evaluated dataset, Y_i is an element of the reference dataset, and $\overline{Y_i}$ is the average for the reference dataset.

3.2.2 Precipitation anomaly and spatial trend before and after the impoundment

The precipitation changes in the TGRA comprised two parts. The first part was caused by local land surface and atmosphere changes. The second part was due to large-scale climate impacts, such as El Niño or interdecadal oscillations (Dai et al., 2015; Dong and Dai, 2015; Trenberth et al., 2002). To analyze the precipitation variations associated with the TGP, the effect of the TGP from large-scale climate impacts should be separated. We used methods described in previous studies (Song et al., 2017; Wu et al., 2006; Zhou et al., 2012) in selecting a regional background to reflect the large-scale climate. In our study, the regional background was defined as the 1° spatial buffer from the TGRA (27.5°N–32.8°N, 104.8°E–112.7°E, as shown in Figure 1), which is consistent with the background region used by Wu et al (2006). The effects of large-scale climate impacts were considered to be similar in the TGRA and its surrounding region. Therefore, we removed the large-scale climate impacts by subtracting the mean precipitation for the regional background of each month. After the above subtraction, a new time-series of precipitation anomaly was obtained to investigate the variations caused by local changes.

Precipitation characteristics can be extracted based on the new time-series of precipitation anomaly. To highlight the influence on reservoir impoundment, the study was divided into two periods: the pre-impoundment period (1988–2002) and the post-impoundment period (2003–2017).

The Theil–Sen trend estimation method was used in this study Sen's slope quantitatively assesses linear trends, as shown as follows:

$$\beta = Median\left(\frac{x_j - x_i}{j - i}\right) \quad (3)$$

where $1 < i < j < n$, n is the size of the time series, and x_j and x_i are the time-series data of the trend to be analyzed. The positive slope represents an increasing trend, whereas the negative slope indicates a decreasing trend.

As the precipitation in the TGRA is usually concentrated in the summer, the spatial pattern of precipitation in different seasons is distinct. We divided a year into two periods. May–October belongs to the flood season, January–April and November–December compose the dry season.

3.2.3 Concentrated characteristics of precipitation

To analyze the concentration characteristics of precipitation distribution in one year, the PCD and PCP defined by Zhang et al. (2003) were used to represent the distribution characteristics of precipitation over time. Previous studies have shown that PCD and PCP methods can quantitatively reveal the non-uniformity of precipitation in the time field (Chatterjee et al., 2016; Dourado et al., 2013; Silva and Lucio, 2015).

The fundamentals for calculating the PCD and the PCP are based on the vector of monthly total precipitation. The assumption is that monthly total precipitation is a vector quantity with both magnitudes and that the direction for a year can be seen as a circle (360°). Then, the yearly PCP and PCD for a location can be defined as follows:

$$PCD_i = \frac{\sqrt{R_{xi}^2 + R_{yi}^2}}{R_i} \quad (4)$$

$$PCP_i = \arctan(\frac{R_{xi}}{R_{yi}}) \quad (5)$$

$$R_{xi} = \sum_{j=1}^{N} r_{ij} * \sin\theta_j \quad R_{yi} = \sum_{j=1}^{N} r_{ij} * \cos\theta_j \quad (6)$$

where i is the year (i =1988, 1989, …, 2017), j represents the hou (a year is divided into 72 hou) in a year (j =1, 2, …, 72), r_{ij} denotes total precipitation in the jth hou in the ith year, θ_j is the azimuth of the jth hou, and R_i is the total precipitation of the station in year i.

3.2.4 Cross-wavelet transform (CWT) analysis

Hydrometeorological time series has characteristics of randomness, ambiguity, nonlinearity, non-stationarity, and multiple time scales. CWT can analyze the time–frequency domain fluctuations of two mutually coupled time series based on wavelet transform. Using CWT decomposition of hydrometeorological data for multiscale analysis has been widely used in recent years (Deng et al., 2018; Yang et al., 2020).

In this study, we explored the possible relationships between precipitation anomaly and monthly average water level by CWT analysis. Grinsted et al. (2004) described the specific algorithm in detail. The MATLAB CWT toolbox can be download from GitHub (available at https://github.com/grinsted/wavelet-coherence).

4 Results and discussion

4.1 Evaluation of precipitation data

Figure 2 shows the scatter diagram of 360 monthly from January 1988 to December 2017 between station observation data and different datasets. The CC among the three datasets and the observation data of the stations were all above 0.85. CN05.1 had the highest CC (0.94), whereas the 1-km dataset had the lowest CC (0.85). In comparison with different datasets, the 1-km dataset had the highest RMSE (38.36 mm), whereas CN05.1 had the smallest RMSE (26.99 mm).

To further analyze the accuracy of the three datasets in the 1° buffer zone of the TGRA, we calculated the CC and RMSE among the three datasets and the observation data in different months during the study period. Table 1 shows the results. CN05.1 provided the most reliable precipitation data in most months of the year during the study period.

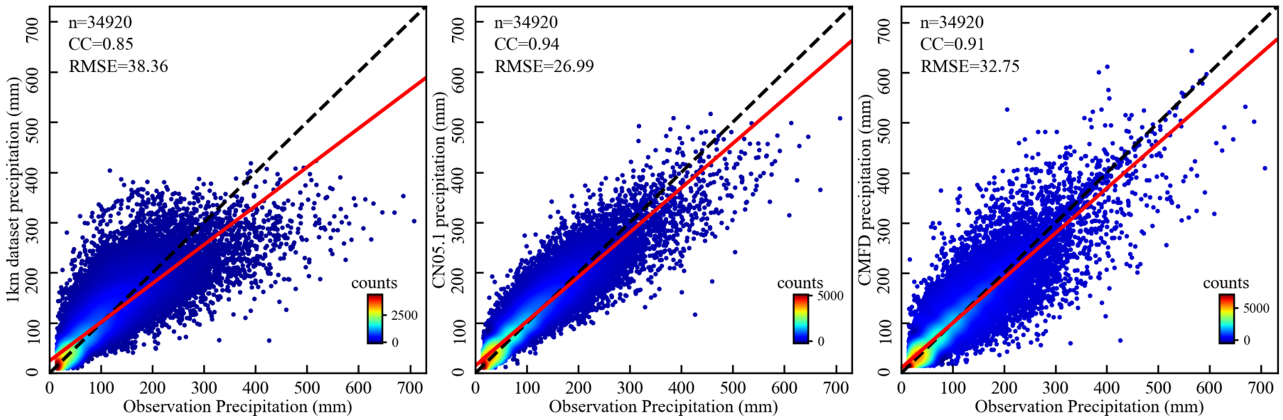

Figure 2. Scatter plot of precipitation from (a) 1-km dataset, (b) CN05.1, and (c) CMFD and station observations with linear least squares fit (red line).

Table 1. Statistical metrics summarizing the performance of monthly precipitation estimates based on different datasets relative to station observations (unit: mm/month for monthly data)

	CC			RMSE		
Time	1KM dataset	CN05.1	CMFD	1km dataset	CN05.1	CMFD
Jan	0.77	0.89	0.66	9.29	6.43	14.15
Feb	0.88	0.94	0.83	10.96	8.07	14.03
Mar	0.74	0.89	0.77	17.51	11.88	19.91
Apr	0.75	0.91	0.87	31.84	20.48	24.08
May	0.69	0.86	0.82	42.17	30.27	34.80
Jun	0.60	0.85	0.82	64.23	42.63	47.99
Jul	0.63	0.86	0.82	80.90	53.74	60.54
Aug	0.68	0.86	0.81	64.94	45.75	52.97
Sept	0.75	0.90	0.86	51.03	33.42	36.75
Oct	0.77	0.91	0.84	27.22	18.85	24.15
Nov	0.80	0.93	0.84	19.92	11.97	18.89
Dec	0.77	0.90	0.67	8.86	5.84	12.36

Figure 3 shows the spatial distributions of annual mean precipitation over 1988–2017 from different datasets and station observations. All the three grid datasets reflected the main spatial characteristics of the annual mean precipitation field in the 1° buffer zone of the TGRA. The precipitation was more in the south-central part and less in other areas. However, in some areas, the spatial distribution of CN05.1 and CMFD data was more consistent with the station data, especially over the vicinity of (29N, 105E). The CN05.1 and CMFD datasets objectively reflected the characteristics of less precipitation in the region. Conversely, the 1-km dataset smoothed out the extreme value center of the regional precipitation, in which accurately describing the local precipitation characteristics of the reservoir area is difficult.

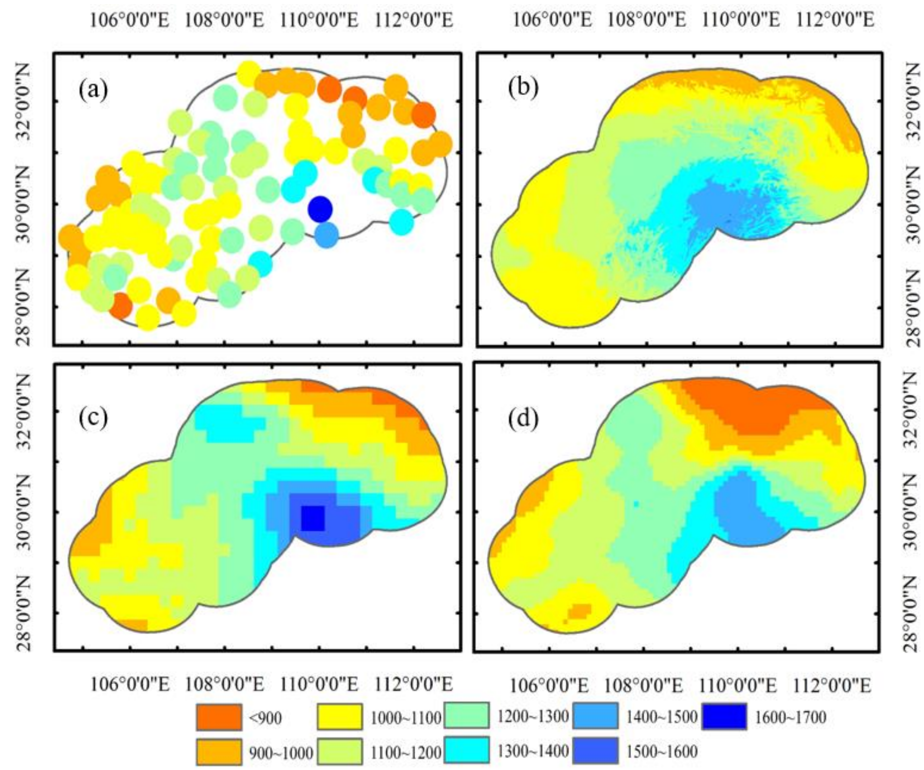

Figure 3. Spatial distribution of annual mean precipitation over 1988–2017 from (a) station observations, (b) 1-km dataset, (c) CN05.1, and (d) CMFD (unit: mm/yr).

According to the results, the precipitation distributions based on CMFD and CN05.1 were generally similar. CN05.1 and CMFD could accurately reflect the spatial characteristics of precipitation in the TGRA. In terms of average monthly precipitation for different months, the difference between CN05.1 and station observations was smallest in comparison, followed by CMFD and then the 1-km dataset. Thus, CN05.1 data were selected to study the precipitation changes in 15 years before and after the impoundment of the TGP.

4.2 Analysis on the variation of precipitation anomaly and its spatial trend

Figure 4 displays the annual and seasonal precipitation anomaly in the TGRA from 1988 to 2017. The annual precipitation anomaly showed an increasing trend during the whole study period, with a linear trend of 0.40 mm/yr, but has not passed the significance test (ρ value < 0.05). The maximum precipitation anomaly was 139.24 mm, which was in 2017. The minimum precipitation anomaly was −68.60 mm and occurred in 2010. The precipitation anomaly in the flood season during the study period had a decreasing trend (Figure 4(b)), with a linear trend of −0.15 mm/yr, the linear trend has not passed the significance test (ρ value < 0.05). The maximum value of precipitation anomaly occurred in 2017, which was 121.65 mm. The minimum value was −75.02 mm in 2010. The maximum and minimum values of precipitation anomaly in the flood season occurred in the same year as the annual precipitation anomaly, and the precipitation anomaly in the flood season could explain most of the annual precipitation anomaly in the two years. The decrease of precipitation in the flood season may be caused by the slow heating up of a large quantity of water areas in summer, resulting in the reduction of ascending convection. Moreover, drainage in the TGRA was mainly conducted in the flood season. The drainage would reduce the water area and change the humidity over the TGRA. These will lead to the decrease of precipitation (Miller et al., 2005).

Figure 4(c) shows the change in precipitation anomaly in the dry season. The precipitation anomaly had an increasing trend during the whole study period, with a linear trend of 0.55 mm/yr, but the linear trend has not passed the significance test (ρ value < 0.05). The maximum value of precipitation anomaly was in 2011 (39.03 mm), and the minimum value was in 1990 (-24.82 mm). The impoundment of the TGRA generally began in November, corresponding to the dry season in our study. The measured water level data of the reservoir area from 2003 to 2017 (Figure 5) also showed that the water level in the dry season of the TGRA was significantly greater than that in the flood season. After the water impounding in the TGRA, the water area would increase; this change affected the local water vapor cycle from a small scale (Gao and Fang, 2013) and may be the reason for the increased precipitation anomaly during the dry season.

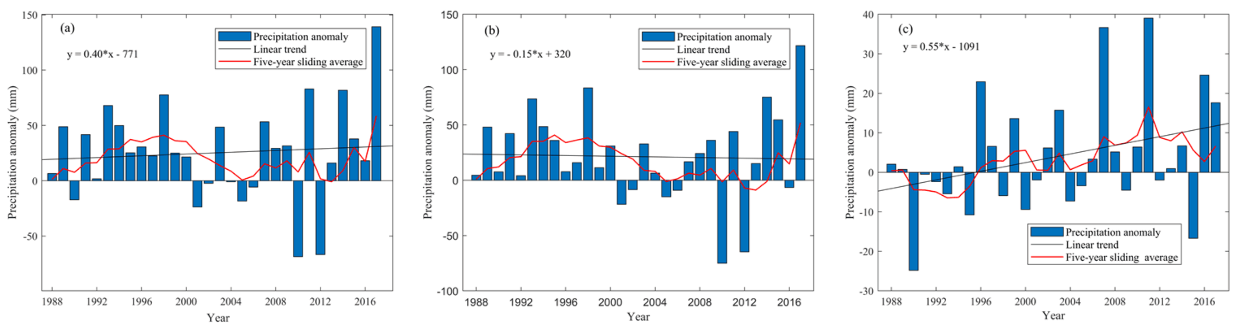

Figure 4. Change in precipitation in the (a) whole year, (b) flood season, and (c) dry season in the TGRA from 1988 to 2017.

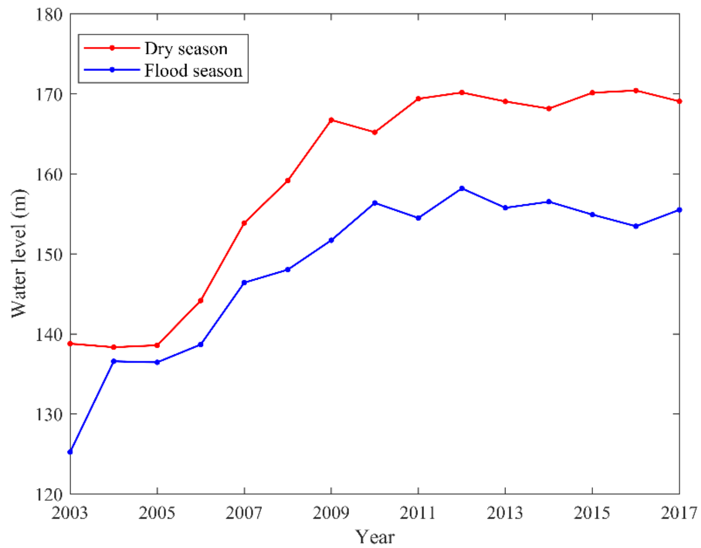

Figure 5. Variation of monthly average water level in dry and flood seasons from 2003 to 2017 in the TGRA.

Figure 6 shows the time series of monthly precipitation anomaly before and after the impoundment. The result shows that July was the largest precipitation anomaly before and after the impoundment difference among all months in the year. The precipitation was 11.74 mm less than that before the impoundment. This result is consistent with the decreasing trend of the precipitation anomaly in the flood season analyzed in the previous section. July was the month with the most precipitation in the Yangtze River Basin, but the average precipitation anomaly in July was the smallest in all months in the year after the impoundment. Impoundment and drainage affected the precipitation anomaly in the TGRA.

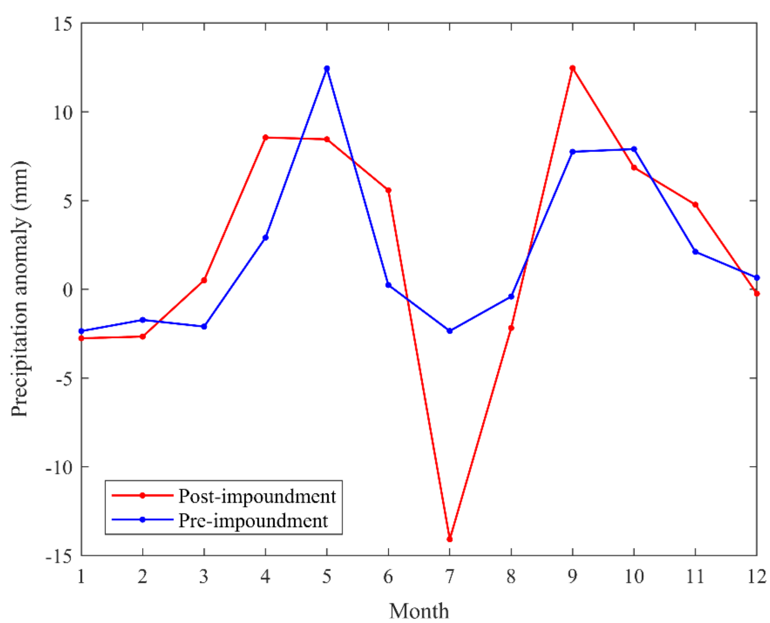

Figure 6. Monthly precipitation anomaly before and after the impoundment in the TGRA.

Figure 7 displays the spatial distribution of annual and seasonal precipitation anomaly trends before and after the impoundment in the TGRA. As shown in Figure 7(a)–7(c), the annual and flood season precipitation anomaly decreased in the area between Badong and Fengjie Stations before the impoundment. The region near Yichang Station showed a trend of becoming wet. The precipitation anomaly in the dry season before the impoundment did not show a clear trend.

As shown in Figure 4(b), although the precipitation anomaly in flood season showed a decreasing trend from 1988 to 2017, the precipitation anomaly showed an increasing trend from 2003 to 2017. Therefore, after impoundment, the spatial distribution of annual, flood season, and dry season precipitation anomaly was dominated by an increasing trend. Figure 7(d)–7(f) demonstrate that in the annual, flood season, and dry season, precipitation anomaly around the TGD showed a different increasing trend, especially in the area between Badong and Fengjie Stations. The precipitation anomaly also greatly changed in the southern part of Fengdu Station in the upper reaches of the TGRA, which decreased after the impoundment in the annual, flood season, and dry season. No obvious change was observed in other regions before and after the impoundment.

Overall, the region near the dam shows the largest variation in precipitation anomaly, which may be related to the largest variation of water area around the dam. The precipitation in the flood season was higher than that in the dry season. Therefore, the change pattern of annual precipitation anomaly was mainly affected by the change in precipitation in the flood season. In the dry season, the main change was that precipitation anomaly decreased in the west and increased in the east after the impoundment. The changes were smaller than that in a whole year and the flood season.

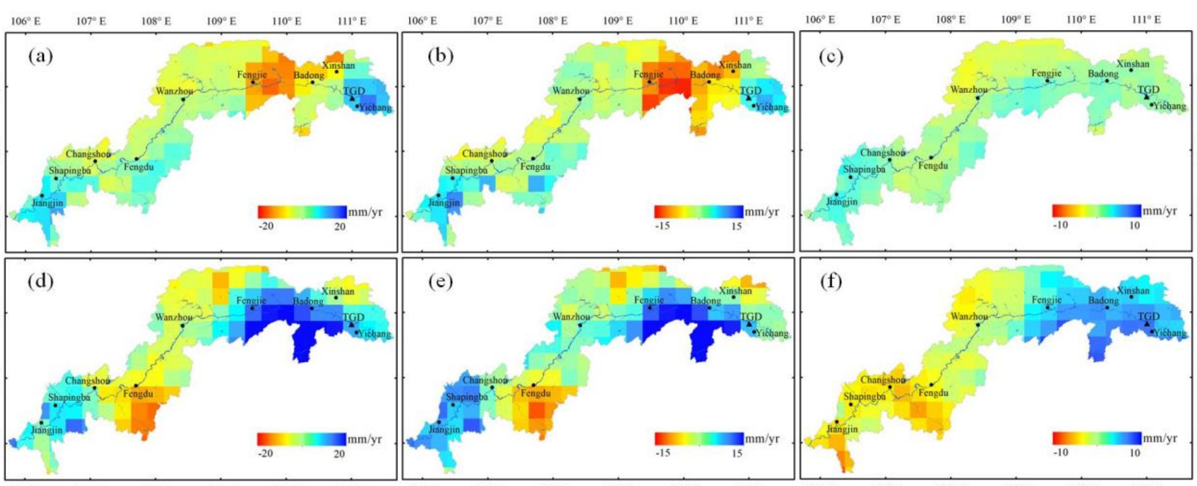

Figure 7. Distribution of precipitation anomaly trends before the impoundment in (a) a year, (b) the flood season, (c) the dry season, and after the impoundment in (d) a year, (e) the flood season, and (f) the dry season.

4.3 Variation of PCD and PCP in the TGRA

4.3.1 Time-series variation of PCD and PCP

Figure 8 shows the interannual variations of PCD and PCP in the TGRA from 1988 to 2017. In the TGRA, the average PCD value over the years was 0.45 (Figure 8(a)). The interannual changes were drastic. The minimal value for the whole study period was 0.28 (in 2001). The maximal value of PCD was 0.54 (in 1998). The PCD values change obviously in different stages. From 1988 to 2002, the average value of PCD was 0.48. PCD fluctuated greatly, and the standard deviation (STD) is 0.07. The change is more stable from 2003 to 2017, the average value of PCD is 0.42, and the STD is 0.05. The precipitation become more even than that before the impoundment. For the whole study period, the years with high PCD values are 1988, 1991, 1998, and 2003; and the years with low PCD values are 1989, 2001, and 2016. Generally, the years with high precipitation anomaly always had a high PCD value, and serious flood disasters would then occur in the TGRA, such as the catastrophic flood disaster in the Yangtze River Basin in 1998. If the years have a high precipitation anomaly but with low PCD value, then flood disasters are less likely to happen.

The annual mean of PCP is 37.49 in the TGRA (Figure 8(b)), mainly concentrated in mid-July. The minimal value was 32.61 (in 1990), and the maximal value was 41.82 (in 2000). PCP showed similar changes with PCD. The STD of PCD was 2.72 in the pre-impoundment and 2.24 in the post-impoundment. Thus, the value changed sharply before the impoundment. After the impoundment, the value of PCP fluctuated slightly. The average value of PCP in the pre-impoundment was 37.38. The average value in the post-impoundment was 37.59. Thus, PCP was delayed relative to that before the impoundment.

Before the TGD was put into operation, the precipitation in the Yangtze River Basin was mainly concentrated in the flood season, less in the dry season. As mentioned previously, after the TGD was utilized, precipitation showed an increasing trend in the dry season and a decreasing trend in the flood season. After the impoundment, the average value of PCD in the TGRA was lower than that before the impoundment, and the precipitation distribution was more uniform. The average value of PCP in the TGRA was higher than that before the impoundment, and PCP was delayed.

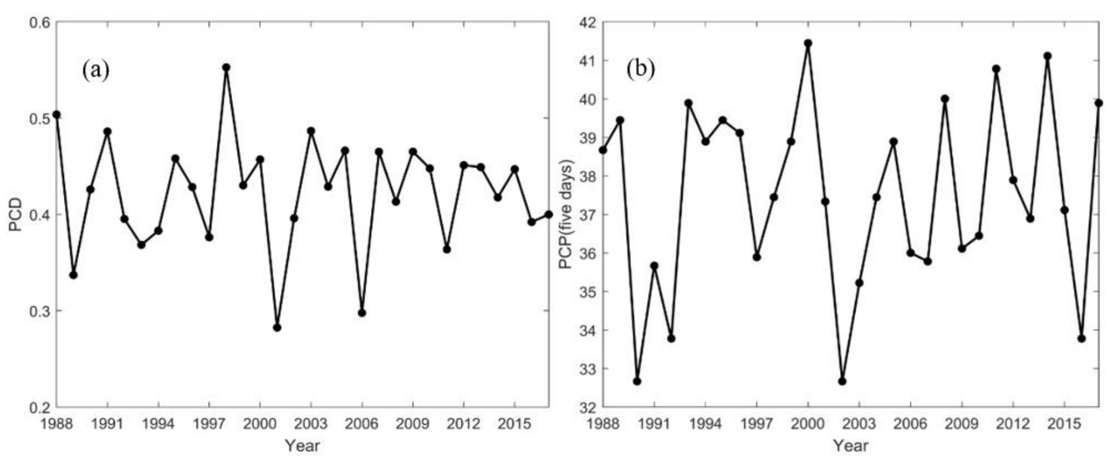

Figure 8. Interannual variation of (a) PCD and (b) PCP in the TGRA from 1988 to 2017.

4.3.2 Spatial pattern of PCD and PCP in the TGRA

Figure 9 reveals the spatial distribution of PCD and PCP in the TGRA before and after the impoundment from 1988 to 2017. Figure 9(a)–9(c) show that the PCD of the TGRA varied between 0.34 and 0.50 during the whole study period. The areas with larger PCD were mainly concentrated in the downstream of the TGRA. The comparison between Figure 9(b) and 9(c) shows that the PCD varied greatly along the downstream basin below Wanzhou Station before the impoundment. The PCD ranged from 0.42 to 0.46 after the impoundment. The area of PCD increase was mainly in the north of the downstream of the TGRA. The area where PCD showed a decreasing trend was mainly around Fengdu Station.

In Figure 9(d)–9(f), the PCP showed a decreasing trend from north to south during the whole study period. During the entire study period, the PCP of the TGRA was mainly between 35 hou and 39 hou. The PCP before the impoundment was between 34 hou and 39 hou. After the impoundment, the PCP in most areas was delayed by 1 hou to 2 hou compared with that before the impoundment. The obvious change was that the area in the TGD and around Yichang Station were delayed from 37 hou to 38 hou after the impoundment. The middle and northern of the TGRA was postponed from 37 hou to 39–40 hou after the impoundment.

On the basis of the above analysis, the PCD and PCP show two important characteristics. (1) Obvious banding distribution existed. (2) The contour line was basically in the direction of north–south. The PCD varied obviously in different seasons. The PCD in the northeast was relatively large, and the PCD and PCP changed greatly in the region near the TGD. The PCD and PCP also changed greatly before and after the impoundment.

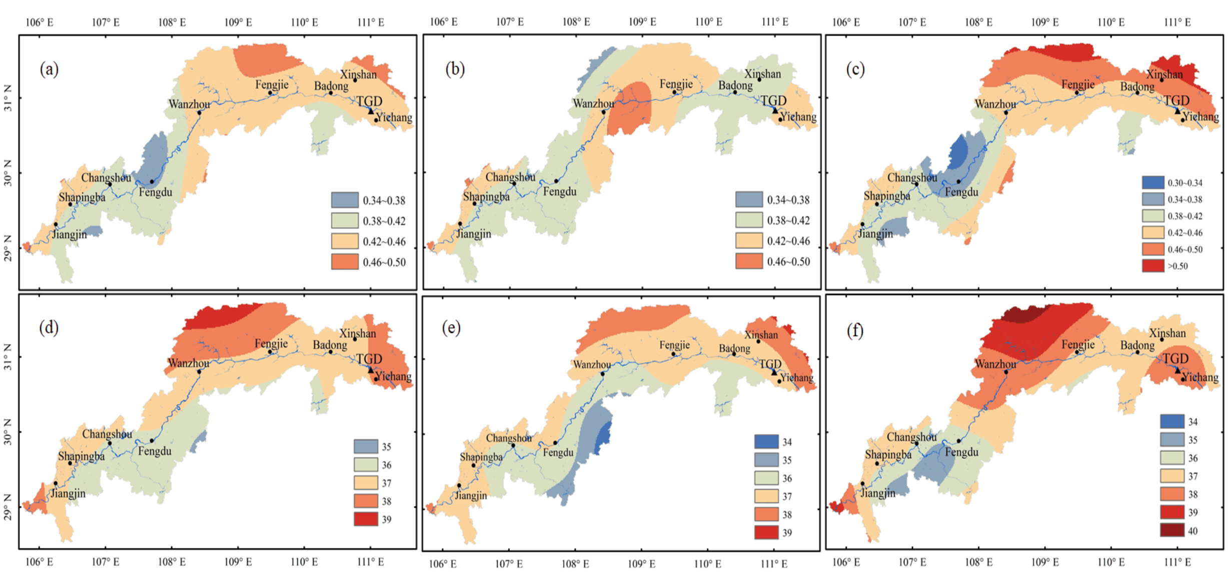

Figure 9. Spatial distribution of (a) PCD from 1988 to 2017, (b) PCD before the impoundment, (c) PCD after the impoundment, (d) PCP from 1988 to 2017, (e) PCP before the impoundment, and (f) PCP after the impoundment in the TGRA.

4.4 Relationship between precipitation anomaly and water level

To further explore the influence of the TGP on the variation of regional precipitation anomaly, CWT analysis was performed on the monthly precipitation anomaly and the monthly average water level. Figure 10(a) shows the cross-wavelet power between precipitation anomaly and monthly average water level in the TGRA. The phase vector rightward horizontal arrow denotes 0°, indicating that the peak water level corresponds to a simultaneous increase in precipitation anomaly. The leftward horizontal arrow denotes 180°, indicating that the peak water level corresponds to a decrease in precipitation anomaly. Figure 10(a) shows that the monthly average water level and the monthly precipitation anomaly in the TGRA mainly exhibited significant resonance phenomenon after 2011. Moreover, resonance periods of 11–12 months and 10–14 months occurred, and the 95% red noise test was passed. The resonance period of 11–12 months was significant from 2011 to 2013, and the phase difference indicated that the monthly average water level was approximately positively correlated with the precipitation anomaly. Similarly, our study suggests that that precipitation anomaly had a positive correlation with the monthly average water level at the 10–14 month scale from 2014 to 2016. The phase difference indicated that the water level change was ahead of the precipitation anomaly change.

Figure 10(b) shows the corresponding wavelet coherence between precipitation anomaly and monthly average water level in the TGRA. It also demonstrates that the monthly average water level and monthly precipitation anomaly exhibited resonance phenomenon after 2010. The energy spectrum shows that the resonance periods were 12 months (2011–2012) and 5–7 months (2011–2014).

The monthly average water level and precipitation anomaly in the TGRA exhibited an obvious resonance phenomenon after 2011 (Figure 10). The relationship between the average water level and precipitation anomaly mainly exhibited a positive correlation. The influence of water level on precipitation anomaly in the TGRA mainly concentrated in the higher frequency, which was more obvious after 2011. The 175 m of experimental water storage in the TGRA was started in 2010, which reflects the natural regulation of precipitation in the TGRA by high water level operation.

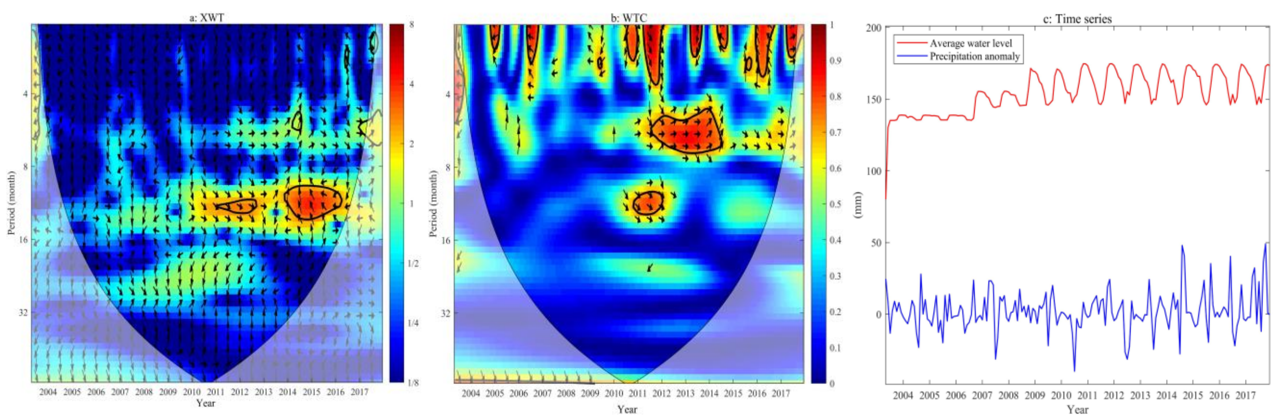

Figure 10. Wavelet coherence between precipitation anomaly and monthly average water level ((a) cross-wavelet power between precipitation anomaly and monthly average water level; (b) corresponding wavelet coherence between precipitation anomaly and monthly average water level).

5 Conclusions

In recent years, the TGP has received attention worldwide, as well as how climate change in the TGRA is the most important aspect. In this study, we used precipitation station data, long time-series meteorological grid data, and water level data to evaluate the climatic impacts of the TGP. The results provide useful information for residents to adapt to local climate change. The main conclusions are as follows.

(1) The accuracy of 1-km dataset, CN05.1 and CMFD in the 1° buffer zone of the TGRA was evaluated by using the site measured data provided by the Hubei Meteorological Bureau. The results showed that the precipitation data of CN05.1 and CMFD were consistent with the annual average precipitation observed by the stations in spatial distribution. However, CN05.1 generally performed better at annual and monthly timescales because it merged observations from more than 2400 stations, which had substantial benefits for the quality of the analysis.

(2) During the study period, the annual precipitation anomaly and the dry season precipitation anomaly showed an increasing trend, while the flood season precipitation anomaly showed a decreasing trend. The areas with a large change were mainly concentrated in the area near the TGD, both of which changed from a decreasing trend to an increasing trend. The precipitation anomaly in April, June, and July had more major changes than that before the impoundment. These changes may be explained by the TGRA storage in the dry season and drainage in the flood season. The impounding caused the water level to rise and the water area to expand. The drainage decreased the water area, which affected the water vapor cycle and resulted in the changes in precipitation.

(3) From 1998 to 2017, the PCD in different areas of the TGRA was quite different. Particularly, the northeast was a high-value area. The PCP showed a banding distribution, where the high-value area was also in the northeast. After the impoundment, the annual PCD and PCP values fluctuated less than before, and the average PCD value decreased. The PCP was delayed in the area around the TGD and Yichang Station. If the PCD is small, the occurrence of flood disasters is not conducive. Thus, the TGP plays a role in flood control.

(4) The CWT analysis indicated that the monthly average water level showed a significant positive correlation with the precipitation anomaly after 2011. No significant resonance phenomenon was found before. This phenomenon indicated that the higher water level may have a greater impact on climate

Our findings are useful for the government and other departments to understand the climate impacts of large hydroelectric projects. In this study, we focus on the relationship between precipitation anomaly and water level. However, after 2003, other factors, such as various climatic factors, forest coverage, vegetation biomass, landscape pattern, and land cover/use, also changed. Future analyses considering more factors may produce further evidence.

References

Abolverdi, J., Ferdosifar, G., Khalili, D., & Kamgar-Haghighi, A. A. (2016). Spatial and temporal changes of precipitation concentration in Fars province, southwestern Iran. METEOROLOGY AND ATMOSPHERIC PHYSICS, 128(2), 181-196, doi: 10.1007/s00703-015-0414-0.

Beatty, S., Allen, M., Lymbery, A., Jordaan, M. S., Morgan, D., Impson, D., Marr, S., Ebner, B., & Weyl, O. L. F. (2017). Rethinking refuges: Implications of climate change for dam busting. BIOLOGICAL CONSERVATION, 209, 188-195, doi: 10.1016/j.biocon.2017.02.007.

Beck, H. E., van Dijk, A. I. J. M., Levizzani, V., Schellekens, J., Miralles, D. G., Martens, B., & de Roo, A. (2017). MSWEP: 3-hourly 0.25 degrees global gridded precipitation (1979-2015) by merging gauge, satellite, and reanalysis data. HYDROLOGY AND EARTH SYSTEM SCIENCES, 21(1), 589-615, doi: 10.5194/hess-21-589-2017.

Chatterjee, S., Khan, A., Akbari, H., & Wang, Y. (2016). Monotonic trends in spatio-temporal distribution and concentration of monsoon precipitation (1901-2002), West Bengal, India. ATMOSPHERIC RESEARCH, 182, 54-75, doi: 10.1016/j.atmosres.2016.07.010.

Dai, A., Fyfe, J. C., Xie, S., & Dai, X. (2015). Decadal modulation of global surface temperature by internal climate variability. Nature Climate Change, 5(6), 555, doi: 10.1038/nclimate2605.

Degu, A. M., Hossain, F., Niyogi, D., Pielke, R. S., Shepherd, J. M., Voisin, N., & Chronis, T. (2011). The influence of large dams on surrounding climate and precipitation patterns. GEOPHYSICAL RESEARCH LETTERS, 38(L04405), doi: 10.1029/2010GL046482.

Deng, S., Chen, T., Yang, N., Qu, L., Li, M., & Chen, D. (2018). Spatial and temporal distribution of rainfall and drought characteristics across the Pearl River basin. SCIENCE OF THE TOTAL ENVIRONMENT, 619, 28-41, doi: 10.1016/j.scitotenv.2017.10.339.

Dong, B., & Dai, A. (2015). The influence of the Interdecadal Pacific Oscillation on Temperature and Precipitation over the Globe. CLIMATE DYNAMICS, 45(9-10), 2667-2681, doi: 10.1007/s00382-015-2500-x.

Dourado, C. D. S., de Medeiros Oliveira, S. R., & Heuminski De Avila, A. M. (2013). Analysis of rainfall homogeneous areas in time series of precipitation in the State of Bahia, Brazil. BRAGANTIA, 72(2), 192-198, doi: 10.1590/S0006-87052013000200012.

Fang, Z., Hang, D., & Xinyi, Z. (2010). Rainfall regime in Three Gorges area in China and the control factors. INTERNATIONAL JOURNAL OF CLIMATOLOGY, 30(9), 1396-1406, doi: 10.1002/joc.1978.

Gao, D., & Fang, C. Y. (2013). The Study on the Relationship of the Poyang Lake Water Level and the Water Area By Using MODIS Data from 2000 to 2012. In: Zhao, J., Iranpour, R., Li, X., & Jin, B., eds. Advanced Materials Research. STAFA-ZURICH: TRANS TECH PUBLICATIONS LTD, pp. 4636-4640, doi: 10.4028/www.scientific.net/AMR.726-731.4636.

Grinsted, A., Moore, J. C., & Jevrejeva, S. (2004). Application of the cross wavelet transform and wavelet coherence to geophysical time series. NONLINEAR PROCESSES IN GEOPHYSICS, 11(5-6), 561-566, doi: 10.5194/npg-11-561-2004.

He, J., Yang, K., Tang, W., Lu, H., Qin, J., Chen, Y., & Li, X. (2020). The first high-resolution meteorological forcing dataset for land process studies over China. Scientific Data, 7(1), doi: 10.1038/s41597-020-0369-y.

Hossain, F. (2010). Empirical Relationship between Large Dams and the Alteration in Extreme Precipitation. Natural Hazards Review, 11(3), 97-101, doi: 10.1061/(ASCE)NH.1527-6996.0000013.

Hu, Z., Zhou, Q., Chen, X., Li, J., Li, Q., Chen, D., Liu, W., & Yin, G. (2018). Evaluation of three global gridded precipitation data sets in central Asia based on rain gauge observations. INTERNATIONAL JOURNAL OF CLIMATOLOGY, 38(9), 3475-3493, doi: 10.1002/joc.5510.

Li, X., Jiang, F., Li, L., & Wang, G. (2011). Spatial and temporal variability of precipitation concentration index, concentration degree and concentration period in Xinjiang, China. INTERNATIONAL JOURNAL OF CLIMATOLOGY, 31(11), 1679-1693, doi: 10.1002/joc.2181.

Li, Y., Zhou, W., Chen, X., Fang, D., & Zhang, Q. (2017). Influences of the Three Gorges Dam in China on Precipitation over Surrounding Regions. Journal of Meteorological Research, 31(4), 767-773, doi: 10.1007/s13351-017-6177-4.

Li, Y., Wu, L., Chen, X., & Zhou, W. (2019). Impacts of Three Gorges Dam on Regional Circulation: A Numerical Simulation. JOURNAL OF GEOPHYSICAL RESEARCH-ATMOSPHERES, 124(14), 7813-7824, doi: 10.1029/2018JD029970.

Manz, B., Buytaert, W., Zulkafli, Z., Lavado, W., Willems, B., Alberto Robles, L., & Rodriguez-Sanchez, J. (2016). High-resolution satellite-gauge merged precipitation climatologies of the Tropical Andes. JOURNAL OF GEOPHYSICAL RESEARCH-ATMOSPHERES, 121(3), 1190-1207, doi: 10.1002/2015JD023788.

Miao, Y., & Wang, A. (2020). A daily 0.25°×0.25° hydrologically based land surface flux dataset for conterminous China, 1961–2017. JOURNAL OF HYDROLOGY, 590, 125413, doi: 10.1016/j.jhydrol.2020.125413.

Miller, N. L., Jin, J. M., & Tsang, C. F. (2005). Local climate sensitivity of the Three Gorges Dam. GEOPHYSICAL RESEARCH LETTERS, 32(L1670416) , doi: 10.1029/2005GL022821.

Niyogi, D., Kishtawal, C., Tripathi, S., & Govindaraju, R. S. (2010). Observational evidence that agricultural intensification and land use change may be reducing the Indian summer monsoon rainfall. WATER RESOURCES RESEARCH, 46(W03533) , doi: 10.1029/2008WR007082.

Peng, S., Ding, Y., Liu, W., & Li, Z. (2019). 1 km monthly temperature and precipitation dataset for China from 1901 to 2017. Earth System Science Data, 11(4), 1931-1946, doi: 10.5194/essd-11-1931-2019.

Silva, B. K. N., & Lucio, P. S. (2015). Characterization of risk/exposure to climate extremes for the Brazilian Northeast-case study: Rio Grande do Norte. THEORETICAL AND APPLIED CLIMATOLOGY, 122(1-2), 59-67, doi: 10.1007/s00704-014-1275-z.

Singh, V., & Qin, X. (2019). Data assimilation for constructing long-term gridded daily rainfall time series over Southeast Asia. CLIMATE DYNAMICS, 53(5-6), 3289-3313, doi: 10.1007/s00382-019-04703-6.

Song, Z., Liang, S., Feng, L., He, T., Song, X., & Zhang, L. (2017). Temperature changes in Three Gorges Reservoir Area and linkage with Three Gorges Project. Journal of Geophysical Research: Atmospheres, 122(9), 4866-4879, doi: 10.1002/2016JD025978.

Sun, B., & Wang, H. (2017). A trend towards a stable warm and windless state of the surface weather conditions in northern and northeastern China during 1961-2014. ADVANCES IN ATMOSPHERIC SCIENCES, 34(6), 713-726, doi: 10.1007/s00376-017-6252-x.

Tang, G., Ma, Y., Long, D., Zhong, L., & Hong, Y. (2016). Evaluation of GPM Day-1 IMERG and TMPA Version-7 legacy products over Mainland China at multiple spatiotemporal scales. JOURNAL OF HYDROLOGY, 533, 152-167, doi: 10.1016/j.jhydrol.2015.12.008.

Trenberth, K. E., Caron, J. M., Stepaniak, D. P., & Worley, S. (2002). Evolution of El Nino-Southern Oscillation and global atmospheric surface temperatures. JOURNAL OF GEOPHYSICAL RESEARCH-ATMOSPHERES, 107(4065D7-8) , doi: 10.1029/2000JD000298.

Wang, J., Chen, H., Xu, C., Zeng, Q., Wang, Q., Kim, J., Chen, J., & Guo, S. (2018). Tracking the error sources of spatiotemporal differences in TRMM accuracy using error decomposition method. Hydrology Research, 49(6), 1960-1976, doi: 10.2166/nh.2018.191.

Wang, Z., Zhong, R., Lai, C., & Chen, J. (2017). Evaluation of the GPM IMERG satellite-based precipitation products and the hydrological utility. ATMOSPHERIC RESEARCH, 196, 151-163, doi: 10.1016/j.atmosres.2017.06.020.

Woldemichael, A. T., Hossain, F., Pielke, R. S., & Beltran-Przekurat, A. (2012). Understanding the impact of dam-triggered land use/land cover change on the modification of extreme precipitation. WATER RESOURCES RESEARCH, 48(W09547) , doi: 10.1029/2011WR011684.

Wu, J., Gao, X., Giorgi, F., Chen, Z., & Yu, D. (2012). Climate effects of the Three Gorges Reservoir as simulated by a high resolution double nested regional climate model. QUATERNARY INTERNATIONAL, 282, 27-36, doi: 10.1016/j.quaint.2012.04.028.

Wu, J., & Gao, X. (2013). A gridded daily observation dataset over China region and comparison with the other datasets. CHINESE JOURNAL OF GEOPHYSICS-CHINESE EDITION, 56(4), 1102-1111, doi: 10.6038/cjg20130406.

Wu, L., Zhang, Q., & Jiang, Z. (2006). Three Gorges Dam affects regional precipitation. GEOPHYSICAL RESEARCH LETTERS, 33(13) , doi: 10.1029/2006GL026780.

Xiao, C., Yu, R., & Fu, Y. (2010). Precipitation characteristics in the Three Gorges Dam vicinity. INTERNATIONAL JOURNAL OF CLIMATOLOGY, 30(13), 2021-2024, doi: 10.1002/joc.1963.

Yang, F., Lu, H., Yang, K., He, J., Wang, W., Wright, J. S., Li, C., Han, M., & Li, Y. (2017). Evaluation of multiple forcing data sets for precipitation and shortwave radiation over major land areas of China. HYDROLOGY AND EARTH SYSTEM SCIENCES, 21(11), 5805-5821, doi: 10.5194/hess-21-5805-2017.

Yang, P., Zhang, Y., Xia, J., & Sun, S. (2020). Investigation of precipitation concentration and trends and their potential drivers in the major river basins of Central Asia. ATMOSPHERIC RESEARCH, 245, 105128, doi: 10.1016/j.atmosres.2020.105128.

Yesilirmak, E., & Atatanir, L. (2016). Spatiotemporal variability of precipitation concentration in western Turkey. NATURAL HAZARDS, 81(1), 687-704, doi: 10.1007/s11069-015-2102-2.

Zeng, Y., Zhou, Z., Yan, Z., Teng, M., & Huang, C. (2019). Climate Change and Its Attribution in Three Gorges Reservoir Area, China. Sustainability, 11(720624) , doi: 10.3390/su11247206.

Zhang, L., & Qian, Y. (2003). ANNUAL DISTRIBUTION FEATURES OF PRECIPITATION IN CHINA AND THEIR INTERANNUAL VARIATIONS. Acta Meteorologica Sinica, 17(02), 146-163, doi: CNKI:SUN:QXXW.0.2003-02-003.

Zhang, X., Tang, Q., Pan, M., & Tang, Y. (2014). A Long-Term Land Surface Hydrologic Fluxes and States Dataset for China. JOURNAL OF HYDROMETEOROLOGY, 15(5), 2067-2084, doi: 10.1175/JHM-D-13-0170.1.

Zhang, Y., Hong, Y., Wang, X., Gourley, J. J., Xue, X., Saharia, M., Ni, G., Wang, G., Huang, Y., Chen, S., & Tang, G. (2015). Hydrometeorological Analysis and Remote Sensing of Extremes: Was the July 2012 Beijing Flood Event Detectable and Predictable by Global Satellite Observing and Global Weather Modeling Systems? JOURNAL OF HYDROMETEOROLOGY, 16(1), 381-395, doi: 10.1175/JHM-D-14-0048.1.

Zheng, L., Xu, J., Tan, Z., Xu, G., Xu, L., & Wang, X. (2020). A thirty-year Landsat study reveals changes to a river-lake junction ecosystem after implementation of the three Gorges dam. JOURNAL OF HYDROLOGY, 589(125185) , doi: 10.1016/j.jhydrol.2020.125185.

Zhou, L., Tian, Y., Roy, S. B., Thorncroft, C., Bosart, L. F., & Hu, Y. (2012). Impacts of wind farms on land surface temperature. Nature Climate Change, 2(7), 539-543, doi: 10.1038/NCLIMATE1505.